ORIGINAL PAPER

Energetic particles' fluxes and dose in the Radiation Gene Box measured by space radiation detector onboard SJ-10 satellite

Xingzhu Cui[1] · Yaqing Liu[1] · Wenxi Peng[1] · Jinzhou Wang[1] · Min Gao[1] · Dongya Guo[1] · Xiaohua Liang[1] · Ruirui Fan[1] · Huanyu Wang[1] · Yunlong Zhang[1,2] · Zhongjian Ma[1] · Mingyang Yan[1] · Hong Xiao[3] · Yuanda Jiang[4] · Haiying Hang[5]

Abstract

Background To evaluate the hazard of space radiation posing to the tissues, it is important to obtain exact fluxes of different radiation particles. The Radiation Gene Box (RGB) onboard SJ-10 spacecraft was an instrument designed to investigate the effects of space environment on the mESCs and drosophila. To derive the dose received by the tissues inside the RGB, the Space Radiation Detector (SRD) was installed inside it.

Purpose The SRD was designed to derive the fluxes of electron, proton, hellion and gamma rays around it. If the type of the particles, the energies, the fluxes and the conversion coefficients are known, the dose received by the tissues could be evaluated.

Methods The SRD was designed as a ΔE-E solid-state telescope. By measuring the energy deposited in the three subdetectors, the particles' type and their energies could be discriminated. The data of SRD were divided into 15 bins by the types of particles and their energy ranges.

Results The gamma ray flux was higher than any other particle flux inside the RGB, and the electron was the most intense charge particle, while the helium ion was the most harmful radiation to the cells inside the RGB.

Conclusion The dose rate inside the Radiation Gene Box was much higher than in the ground, but the integral dose of 12 days inside the RGB was about 2.13 mSv. It seemed unlikely to have obvious biological effects on the tissues of mice and drosophila.

Introduction

The radiations in space have many adverse effects on satellite missions, such as degrading satellite components, giving rise to background noise in detectors, causing errors in digital circuits, inducing electrostatic charge-up in insulators, posing a threat to astronauts. It is a conventional means to research the space radiation environment by measuring fluxes of radioactive particle. Over the past few decades, a batch of particle detectors had been launched and operated in space [1–5], and much valuable data which are useful for evaluating the space radiation effects on the biological issues, electronic equipment had been obtained. Particle detectors had been also adapted in space weather monitor and other scientific studies. The space radiation measurement had been applied to a variety of scientific researches, as shown in Table 1.

The Rad Gene Box (RGB) experiment concerned the following three aspects: (1) To perform the experiment both onboard the SJ-10 satellite and on the ground using the same instrument to know the effects of space environment (including microgravity and space radiation) on the mESCs. (2) To observe the DNA damage response of radioactive sensitive cell mRad9−/− mESCs and to compare with the wild-type

✉ Xingzhu Cui
  cuixingzhu@ihep.ac.cn

[1] Institute of High Energy Physics, CAS, Beijing, China

[2] College of Physics, Jilin University, Changchun, China

[3] Changzhou Institute of Technology, Changzhou, China

[4] National Space Science Center, CAS, Beijing, China

[5] Institute of Biophysics, CAS, Beijing, China

Table 1 The comparison of scientific goals and performances of space radiation detectors

Instrument	Launching time	Performance	Goals
SAC-C/ICARE	2000.11	Electron: 0.25–1.5 MeV Proton: 10–30 MeV Helion: >70 MeV	Measure the space radiation and it effects
INTEGRAL/SREM	2002.10	Electron: 0.55–2.3 MeV Proton: 11–120 MeV Heavy ion: 150–185 MeV/n	Continually measures electron and proton fluxes along the orbit and provides alert information to the spacecraft and payload, support in tracing the spacecraft anomalies
DEMTER/IDP	2004.6	Electron: 70–2500 keV	Systematically study the electromagnetic waves linked to human activities and natural phenomena like earthquakes, volcano eruptions, atmospheric and magnetic storms. Study the related ionospheric changes, and the related precipitation of particles from the radiation belts
RESURS/ARINA	2005.09	Electron: 3–30 MeV Proton: 30–100 MeV	Monitor the bursts of high-energy charged particles as earthquake precursors
PROBA-V/EPT	2013.5	Electron: 0.5–20 MeV Proton: 9.5–248 MeV Helion: 36–1000 MeV	Perform the absolute measurements required for scientific studies

Table 2 Channels of the radiation particles of SRD

Particle type	Energy range (Mev)	Particle bin name
Gamma ray	0.5–2	G
Electron	0.5–10	E1–E3
Proton	5–200	P1–P8
α particle	30–300	A1–A3

mESCs, expecting to observe more significant effects of space environment in mRad9−/− mESCs than that in wild-type mESCs. (3) To find the time-dependent repair delay effect on DNA double-strand breaks induced by radiation in microgravity environment in space, the SRD installed inside the RGB was designed to derive the fluxes of radiation particles such as gamma rays, electrons, protons and α particles, which would produce radiation damage to the tissues cultured in the RGB.

The SJ-10 satellite was launched on 6 April, 2016 to a LEO orbit (235 km Perigee, 269 km apogee, 43° inclination). The data of SRD were divided into 15 bins by the types of particles and their energy ranges [6]. Table 2 provides information concerning the kinds of particles that can be recorded by this detector. The time resolution of SRD is 10 s.

Using the data of SRD, the particles flux inside the RGB and absorbed radiation dose of tissues can be calculated. The effect of space radiation on the tissues can also be assigned.

Instrument

To be able to measure the fluxes, spectra and elemental composition of the main particles inside the RGB, the SRD was designed as a ΔE–E solid-state telescope. The energy loss of charge particle in the detector can be determined by the Bethe formula:

$$\left(-{}^{\mathrm{d}E}/{}_{\mathrm{d}x}\right)_{\mathrm{ion}} \times E \propto MZ^2 \tag{1}$$

where $(\mathrm{d}E/\mathrm{d}x)_{\mathrm{ion}}$ is the energy loss per unit distance, M is the mass of incident particle, Z is the charge of incident particle, while E is energy of the incident particle. The measure to discriminate the particles by the energy deposited in the three sub-detectors had been described by Liu et al. [6].

As shown in Fig. 1, the SRD apparatus was composed of three parts, which are the sensor, the cables and the processing electronic. Energy deposited by space radiation in the sensor would be converted to electronic signals and amplified; then, the signals were transferred to the processing electronic through the cables, where they were converted into digital signals and transferred to the payload electric control box.

The sensor was designed as a classical charge particle telescope with three solid-state detectors. The first layer (SD1) was a silicon diode with thickness of 80 micron, followed by the other two layers (SD2 and SD3) which were cadmium zinc telluride (CZT) detectors of 2 mm thickness. The
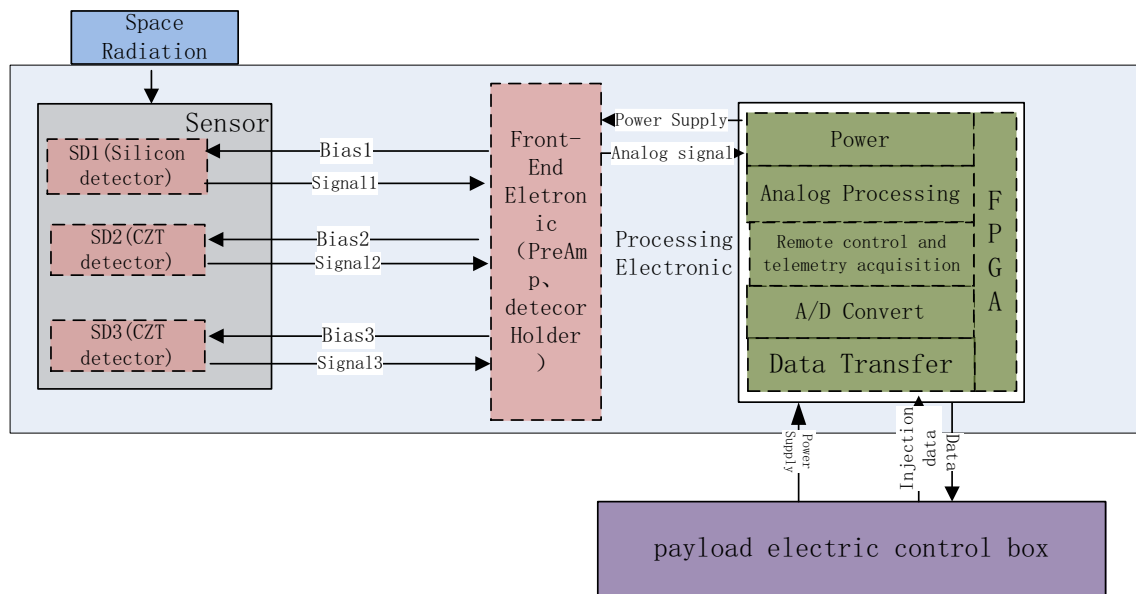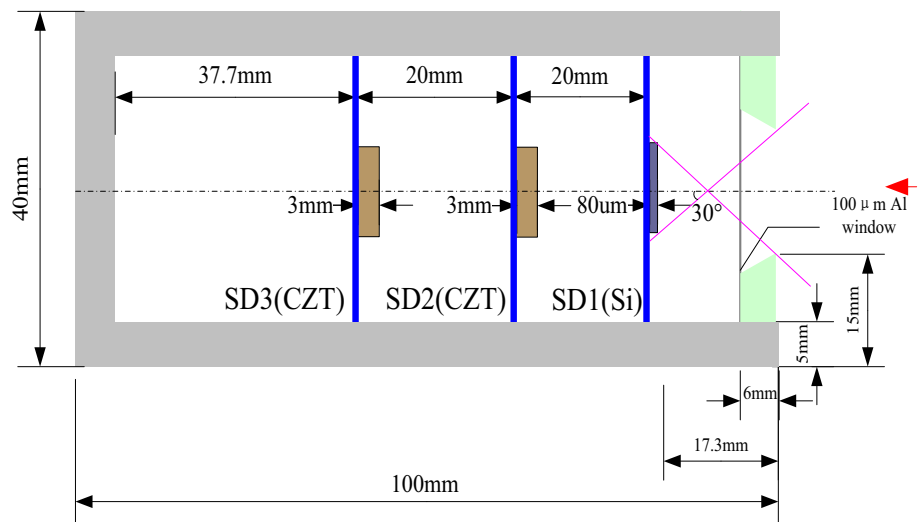
Fig. 1 The schematic diagram of the SRD

Fig. 2 The telescope architecture of the SRD sensor

sensitive areas of all the three detectors were 1 cm². An aluminum foil of 100 micron was placed in front of the first layer as entrance window, which would keep the sensor from interference of visible light and isolate the sensor from the moisture environment inside the RGB. The lower threshold of the incident particle was determined by the material and thickness of window. The distance between the window and the first layer was 11.3 mm. Both the distances between SD1 and SD2 and that between SD2 and SD3 were 20 mm, as shown in Fig. 2.

The solid angles of three sub-detectors were derived by considering both the geometrical factors of the sub-detectors and the energies of charge particles, which were 0.81, 0.33 and 0.33 cm²Sr, respectively.

The cables were designed to supply the biases for the three detectors of the sensor and to transfer the analog amplified signals of the three detectors to the processing electronic. The cables were twisted in pairs to reduce interference effectively.

The processing electronic was consisted of shaping amplifier, ADC, power supply module and FPGA. The amplified signals from the sensors were transformed to Gaussian pulse signals by the shaping amplifier, then the pulse was converted to digital signal by the analog to digital converter (ADC), the digital signals were integrated to a spectrum and stored in the data storage area in FPGA every 10 s, and the data uploading and telemetering were also accomplished by the FPGA.

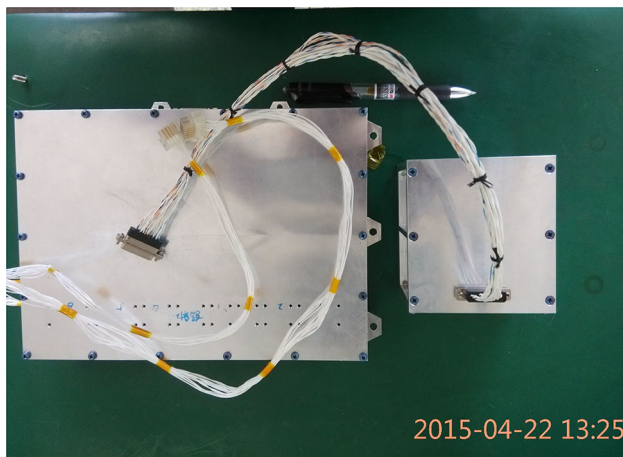The photograph of the three parts described above is shown in Fig. 3.

Fig. 3 The photograph of SRD instrument. The sensor was in the right side, the electronic processing was in the left side, while the two ends of the cables were jointed to the sensor and electronic processing, respectively, with screws

The three sub-detectors were calibrated using ^{241}Am + ^{238}Pu radioactive source before launching to determine the up and low thresholds of them. The calibration results are listed in Table 3.

Observations and data analysis

The observations of SRD had lasted for 12 days since April 6, 2016. The number of obtained spectra was 100,259. The particles' fluxes were derived from the spectra by considering the solid angles of the sensors.

As the radiation flux is pretty low for a single bin defined in Table 2, the fluxes of all the same type of particles were added up into a new bin. To infer the source of the energetic particles, further analysis of the energetic particles' fluxes varying with geomagnetic field was performed. The results showed both the electron distribution and proton distribution had significant inverse relationships with the geomagnetic field, while there was no obvious relationship between the alpha or gamma ray distributions with the geomagnetic field (Figs. 4, 5, 6, 7).

As shown in the figures, the electron and proton fluxes are more intensity in the weak geomagnetic area such as South Atlantic Anomaly (SAA) region, suggesting they are trapped particles by the terrestrial magnetic field. The gamma ray is more intensity at the higher latitude and SAA region, suggesting they were caused by bremsstrahlung effect of charge
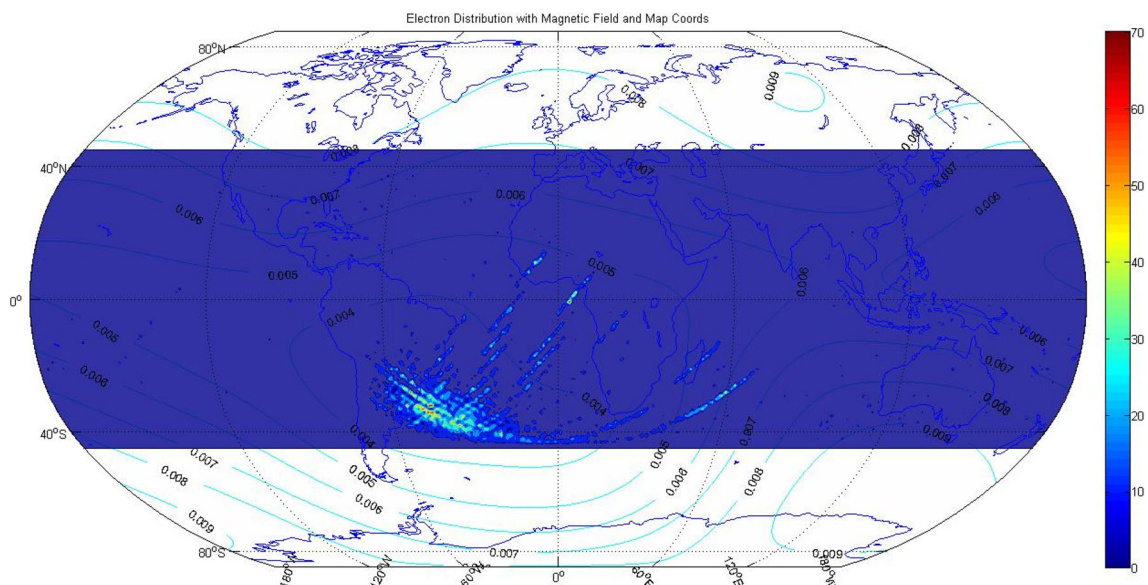
Table 3 The calibration results of the three sub-detectors

Sub-detector	Channel for 5.4 MeV α particle	Voltage for 5.4 MeV α particle	Noise channel	Up threshold[a] (MeV)	Low threshold[b] (keV)
SD1(Si)	680	4.9 V	26	8.13	250
SD2(CZT)	45	0.43 V	1	125	120
SD3(CZT)	58	0.55 V	1	95	93

[a]Corresponding to 10 V voltage which is the maximum output voltage of multi-channel analyzer
[b]Corresponding to pedestal of the energy spectrum

Fig. 4 Mapping of electron fluxes with the magnetic field. The cyan contours are the geomagnetic field contour derived by the World Magnetic Model, while the filled contours are the electron flux derived by the SRD in counts/cm^2/s. The electrons gathered in the low magnetic field region
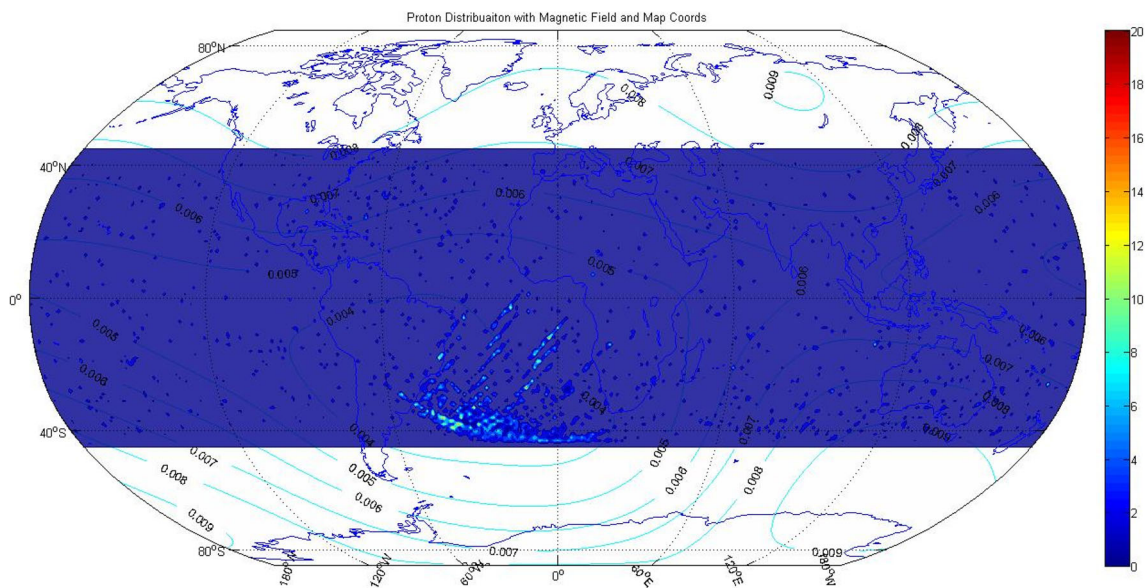
Fig. 5 Mapping of proton fluxes with the magnetic field. The cyan contours are the geomagnetic field contour derived by the World Magnetic Model, while the filled contours are the proton flux derived by the SRD in counts/cm^2/s. The protons also gathered in low the low magnetic field region
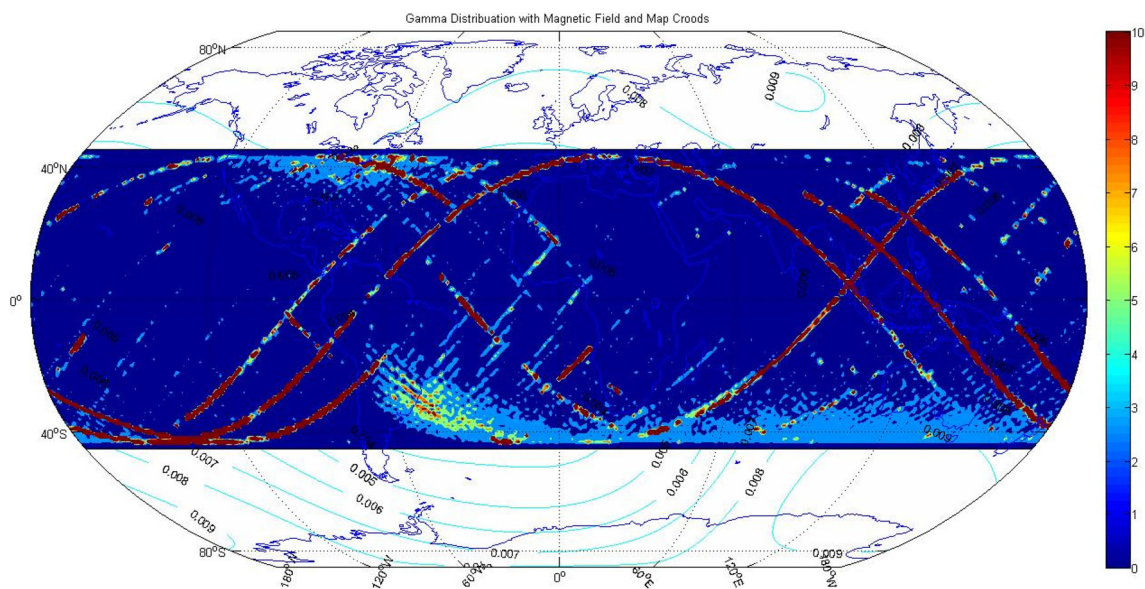

Fig. 6 Mapping of gamma ray with the magnetic field. The cyan contours are the geomagnetic field contour derived by the World Magnetic Model, while the filled contours are the gamma ray flux derived by the SRD in counts/cm^2/s. Gamma rays located mostly at high latitude region

particles. The distribution of alpha is not strictly dependent on the magnetic field strength of geomagnetic, which could be attributable to lesser deflection of alpha particle by in the geomagnetic field due to their larger charge mass ratio (Table 4).

For comparison, both the fluxes of electron measured by SRD and electron flux with the same energy range predicted by AE8 model and the fluxes of proton from SRD and proton flux with the same energy range predicated by AP8 model

are presented in Fig. 8. It can be seen from the figure that the measured fluxes distribution is in good accordance with the model predication (Figs. 7, 8, 9).

To value the damage to the tissues of mice and drosophila, the total dose distribution and the integral dose of all particles were also determined by the particle fluxes and the conversion coefficients for radiological protection quantities for external radiation exposures [7].
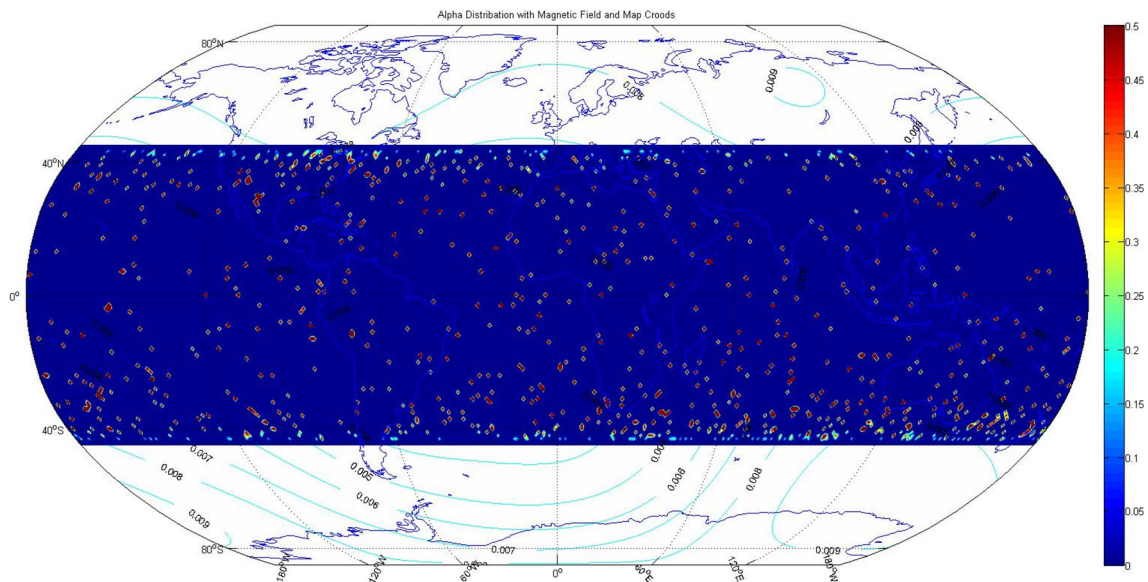
Fig. 7 Mapping of helium ion flux with the magnetic field. The cyan contours are the geomagnetic field contour derived by the World Magnetic Model, while the filled contours are the helium ion flux derived by the SRD in counts/cm^2/s. Helium ion fluxes showed no correlation with the magnetic field

Table 4 The dose of all the particle bins

Particle bin	Total counts[a]	Conversion coefficient[b] (pSv cm^2)	Dose (pSv)
E1 (0.5–1 MeV)	$3,130,909^{+1596}_{-4}$	1.80	$5.63E+6^{+2874}_{-7.2}$
E2 (1–2 MeV)	$33,649^{+17}_{-4}$	4.96	$1.67E+5^{+85}_{-20}$
E3 (2–10 MeV)	$99,461^{+51}_{-2193}$	25.5	$2.54E+6^{+1293}_{-5.59E+4}$
P1 (5–7 MeV)	$48,186^{+1161}_{-37}$	20.5	$9.88E+5^{+2.38E+4}_{-751}$
P2 (7–10 MeV)	$16,731^{+403}_{-41}$	30.67	$5.13E+5^{+1.24E+4}_{-1246}$
P3 (10–15 MeV)	$12,788^{+308}_{-33}$	63.97	$8.18E+5^{+1.97E+4}_{-2088}$
P4 (15–35 MeV)	$378,774^{+9128}_{-33}$	194.09	$7.35E+7^{+1.77E+6}_{-6335}$
P5 (35–50 MeV)	8970^{+216}_{-713}	382.54	$3.43E+6^{+8.27E+4}_{-2.73E+5}$
P6 (50–85 MeV)	$15,444^{+372}_{-1605}$	649.02	$1.00E+7^{+2.42E+5}_{-1.04E+6}$
P7 (85–150 MeV)	$32,399^{+781}_{-6013}$	1395	$4.52E+7^{+1.09E+6}_{+8.39E+6}$
P8 (150–200 MeV)	$58,657^{+1413}_{-967}$	1882	$1.10E+8^{2.66E+6}_{1.82E+6}$
G (0.5–2 MeV)	$5,951,998_{-1853}$	2.46	$1.46E+7^{0}_{-4556}$
A1 (30–60 MeV)	1482^{+738}_{-49}	15,779	$2.34E+7^{+1.17E+7}_{-7.67E+5}$
A2 (60–130 MeV)	$29,942^{+14,920}$	42,337	$1.27E+09^{+6.31E+8}_{0}$
A3 (130–300 MeV)	8578^{+4274}	67,067	$5.75E+08^{+2.87E+8}_{0}$
Total dose (mSv)	$2.13^{-0.94}_{+1.30E-4}$		

Gamma rays located mostly at high latitude region

[a]The systematic uncertainties were calculated from the misjudging rate derived from Geant4 simulation by Liu [8]

[b]The conversion coefficients were taken as interpolations of mean values of the lower limits and upper limits of the energy ranges

As it can be seen from the table, the low energy electron was the most intensity charge particle inside the RGB; however, the helium ion with energy above 60 MeV made more contribution to total dose.

Results

Basing on the discussion above, we could draw a conclusion that the gamma ray flux was higher than any other particle
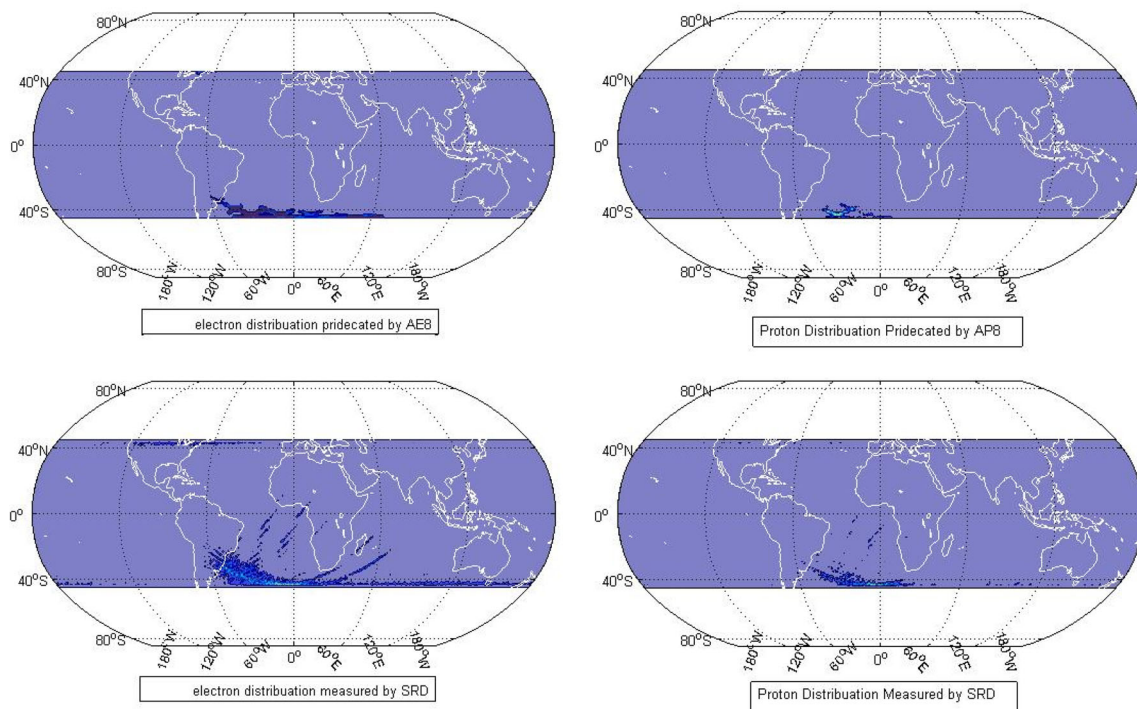
Fig. 8 The comparisons of electron and proton distributions measured by the SRD with those predicted by the AP8 and AE8 model. The left one is the electron comparison, while the right one is the proton comparison
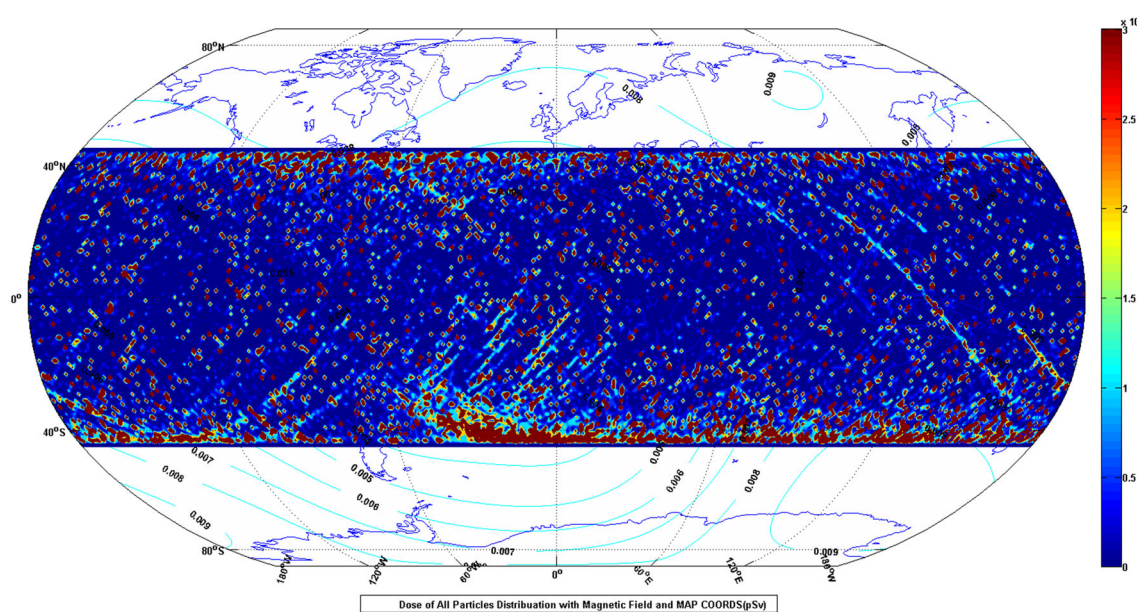

Fig. 9 The distribution of total dose with the magnetic field and map coord. The cyan contours are the geomagnetic field contour derived by the World Magnetic Model, while the filled contours are the total dose in pGy/cm^2

flux inside the RGB, and the electron is the most intense charge particle, while the helium ion was the most harmful radiation to the cells inside the RGB. The dose rate inside the Radiation Gene Box was much higher than the ground, but the integral dose of 12 days inside the RGB was about 2.13 mSv.

It seemed unlikely to have obvious biological effects on the tissues of mice and drosophila.

References

1. D.N. Baker, G.M. Mason, O. Figureoa et al., An overview of the solar, anomalous, and magnetospheric particle explorer (SAMPEX) Mission. IEEE Trans. Geosci. Remote Sens. **31**(3), 531–541 (1993)
2. M. Cyamukungu, S. Benck, S. Borisov et al., The energetic particle telescope (EPT) on board PROBA-V: description of a new science-class instrument for particle detection in space. IEEE Trans. Nucl. Sci. **61**(6), 3667–3681 (2014)
3. J. Labrenz, S. Burmeister, T. Berger et al., Matroshka DOSTEL measurements onboard the International Space Station (ISS). J. Space Weather Space Clim. **5**, A38 (2015)
4. T. Sakaguchi, T. Doke, N. Hasebe et al., LET distribution measurement with a new real-time radiation monitoring device-III onboard the Space Shuttle STS-84. Nucl. Instr. Methods Phys. Res. A **437**(1), 75–87 (1999)
5. G.D. Badhwar, W. Atwell, E.V. Benton et al., A study of the radiation environment on board the Space Shuttle flight STS-57. Radiat. Meas. **24**, 283–289 (1995)
6. Y.Q. Liu, H.Y. Wang, X.Z. Cui et al., Physical design and Monte-carlo simulations of a space radiation detector onboard SJ-10 satellite. Chin. Phys. C **39**, 016002 (2015)
7. C.H. Clement, N. Petoussi-Henss, W.E. Bolch et. al., in *ICRP, 2010. Conversion Coefficients for Radiological Protection Quantities for External Radiation Exposures*. ICRP Publication 116, Ann. ICRP 30(2–5)
8. Y.Q. Liu, Design of space particle detector system onboard SJ-10. Ph.D. thesis, 2014 (**in Chinese**)